

Integrity Fingerprinting of DNN with Double Black-box Design and Verification

Shuo Wang

CSIRO's DATA61 & Cyber CRC

Sidharth Agarwal

Indian Institute of Technology Delhi

Sharif Abuadbba, Kristen Moore, Surya Nepal

CSIRO's DATA61 & Cyber CRC

Salil Kanhere

UNSW

Abstract

Cloud-enabled Machine Learning as a Service (MLaaS) has shown enormous promise to transform how deep learning models are developed and deployed. Nonetheless, there is a potential risk associated with the use of such services since a malicious party can modify them to achieve an adverse result. Therefore, it is imperative for model owners, service providers, and end-users to verify whether the deployed model has not been tampered with or not. Such verification requires public verifiability (i.e., fingerprinting patterns are available to all parties, including adversaries) and black-box access to the deployed model via APIs. Existing watermarking and fingerprinting approaches, however, require white-box knowledge (such as gradient) to design the fingerprinting and only support private verifiability, i.e., verification by an honest party.

In this paper, we describe a practical watermarking technique that enables black-box knowledge in fingerprint design and black-box queries during verification. The service ensures the integrity of cloud-based services through public verification (i.e. fingerprinting patterns are available to all parties, including adversaries). If an adversary manipulates a model, this will result in a shift in the decision boundary. Thus, the underlying principle of double-black watermarking is that a model's decision boundary could serve as an inherent fingerprint for watermarking. Our approach captures the decision boundary by generating a limited number of encysted sample fingerprints, which are a set of naturally transformed and augmented inputs enclosed around the model's decision boundary in order to capture the inherent fingerprints of the model. We evaluated our watermarking approach against a variety of model integrity attacks and model compression attacks. Results show that PublicCheck can detect model integrity breaches with 100% accuracy within five black-box model accesses.

1 Introduction

MLaaS. Cloud-enabled Machine Learning as a Service (MLaaS) has shown enormous promise to transform how deep learning models are developed and deployed. These platforms allow model owners to deploy their pre-trained models and then share them with others (customers) via the API of the cloud platform for profit as a black-box service. Data own-

ers and customers are unaware of the details of the deployed models. Nonetheless, there is a potential risk associated with the use of such services since a malicious party can modify them to achieve an adverse result, such as launching an attack such as a Trojan or backdoor [7, 28, 44, 50], or model compression to save storage space [19]. It is imperative for model owners, service providers, and end-users to verify whether the deployed model has not been tampered with or not.

Existing Landscape. Verifying the integrity of the models can be divided into two broad categories: private verification and public verification. Most of existing verification techniques for model integrity belong to private verifiability and are only available to honest parties, such as *hash values based* [10], *trigger-based* [2] and *sensitive-sample* [19] based watermarking (detailed in Appendix G). (1) *Hash value* based verification is limited because adversaries or dishonest cloud providers may provide unreliable attestation results to customers, leading them to believe that the models are intact when they are not. (2) The essence of *trigger-based* watermarking is to create a backdoor on the target model using a set of trojanized samples that incorporate well-designed triggers into the clean samples, resulting in misclassification to target labels. The predictions on the (trojaned sample, target label) pairs are adopted as the fingerprinting of the model, after fine-tuning the target model with these pairs. As shown in Figure 1, the (trojaned sample, target label) pairs could be considered as a new extension of the classifier's decision boundary as the green line. (3) The essence of the *sensitive-sample-based* watermarking is to produce (adversarial example, target label) pairs as model fingerprinting. Adversarial examples incorporate well-designed noise into the clean samples, resulting in misclassification to target labels. As shown in Figure 1, (adversarial example, target label) pairs could be regarded as singularities on the decision boundary.

Public Verifiability. Private verifiability approaches suffer from the challenges when implemented in public verification scenarios. Towards public verification scenarios in which fingerprinting patterns are available to the public, including adversaries, the following three properties need to be satisfied.

(a) *Practicality.* Public verifiability requires an unlimited number of verifications, but the number of possible verifications is limited by the computational resources available to produce and design fingerprinting patterns. Furthermore, it is important to incorporate randomness and uncertainty into the

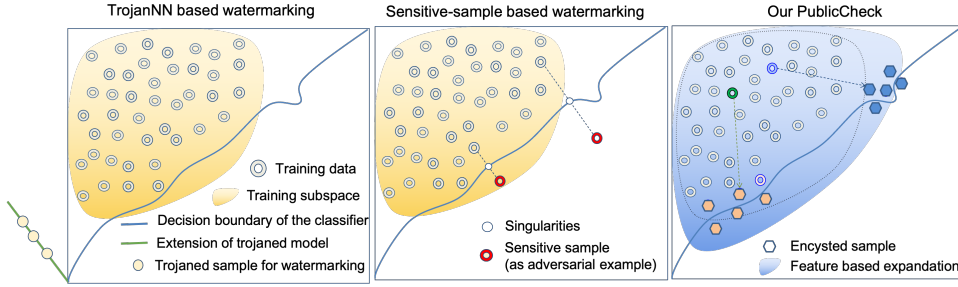


Figure 1: Demonstration of the DNN watermarking.

process of creating fingerprinting patterns.

(b) *Natural for human perception*. An adversary may have access to fingerprinting samples in a public verification scenario. A fingerprinting instance is generally created from an original example by adding a trigger or pixel perturbation. Such pixel-level fingerprinting patterns, however, can be detected, reversed, and then cracked by the attacks, especially when the fingerprint samples can be distinguished by human perception (demonstrated in Figure 11 and 12). Besides, we demonstrate that the detection accuracy of existing fingerprinting approaches, such as Sensitive Sample, sharply decreases when the adversary could perform adversarial training with the recognized fingerprinting samples along with their clean pairs (Section 4.8). To be effective, public fingerprinting must have patterns that are natural for human perception. We consider naturality as a constraint for fingerprinting design.

(c) *Limited knowledge for design*. Existing approaches such as [2, 19] are black-box during the inference while requiring white-box access to the gradient and parameters of the model to design the watermarking samples. However, when the model is non-gradient based or protected, information such as gradients, parameters, or the status of the model in the cloud, are not directly accessible to design the verification mechanisms. The watermarking sample design should accommodate cases where the model’s knowledge is limited, especially when a) the owned model could be encrypted without access to the parameters; b) the owner may only buy the model itself but with very few training samples for the model.

Our Solution. This paper seeks the answers to the following research question: *How to enable MLaaS users to publicly verify the underlying DNN model’s integrity while satisfying the above three properties in black-box settings?* To the best of our knowledge, the proposed PublicCheck is the first practical methodology for public integrity verification with only black-box access to the target MLaaS models during both watermarking design and inference. The intuition is that manipulation of the model will manifest as a shift in the decision boundary, changing the prediction of certain points around the decision boundary. In view of this, the model’s decision boundary could serve as an inherent fingerprint for watermark-

ing. The challenge is how to capture the decision boundary with a limited number of available samples. A possible solution would be to augment the few available data points to be dense around the decision boundary to capture the model’s behavior around the boundary in fine granularity. Generative models are promising methods for such data augmentation, such as GAN [5, 14], VAE [6, 23] and VQVAE [37, 41]. So we define the encysted sample as a set of augmented data points which encyst the classifier’s decision boundary via a generative model, as demonstrated in the last sub-figure of Figure 1. A set of pairs with an encysted sample and its prediction serve as the fingerprint for the model.

Our Contributions. The key contributions are:

(1) We propose a novel Encysted Samples watermarking approach for public integrity verification of DNNs. It only requires black-box access to the MLaaS models through APIs to perform both watermarking design and inference. This approach can be applied to model-agnostic scenarios, with no assumptions on network architecture, hyper-parameters, and training methods.

(2) We develop a feature manipulation generative model to produce unlimited encysted samples for fingerprinting at a low cost, where data samples could be controllably manipulated along a semantic attribute. Randomness and uncertainty are integrated into the generation via latent perturbation, while naturality selection, a metric that correlates with human perception, is used to filter candidate samples, aiming at the imperceptible requirement. In addition, we develop the watermarking sample design to accommodate cases where the model’s knowledge is only black-box or gray-box.

(3) We implement and evaluate our approach against numerous integrity attacks, including model compression of different models (e.g., BadNet, TojanNN, and Clean Label attacks, and model compression of ResNet and VGG-16 models). The results show that our methodology can achieve 100% accuracy on model integrity detection, with zero false-positive rate and low overhead (less than ten black-box model accesses). The naturality evaluation of encysted samples reveals that they are natural for human perception, which is vital for the public verification.

2 Problem Statement and Threat Model

We consider the public verification of models deployed in the cloud to provide prediction services via API, for any user roles, including the model owner, service provider, and any service users. This is a typical MLaaS service provided by service providers, such as Amazon SageMaker. The process of the public verification is illustrated in Figure 2.

The model owner U_M has the trained model f that produces a label for a given input. The verification service starts with the model owner obtaining fingerprints of the models using our PublicCheck methodology before deploying the model to the MLaaS service platform. In general, we make no assumptions about the target model generation process. Given the fingerprinting samples $\{s_i\}_{i=1}^S$, the fingerprint of the model is represented as $\text{FM} = \{(s_i, r_i)\}_{i=1}^V$, $r_i = f(s_i)$, which is produced by the model provider U_M using PublicCheck. Here $V \ll S$ is the minimum number of samples required to conduct efficient verification, and S should be as large as possible to allow for multi-time public verification. A secure server would be appropriate for maintaining PublicCheck model and storing fingerprint samples for public verification. We also provide a fingerprinting images management solution based on blockchain and InterPlanetary File System in Appendix F.

The model is then uploaded and stored on a platform maintained by the cloud vendor U_P , then deployed to an endpoint instance to provide an API querying service for public users. An adversary may compromise a target model since it is uploaded by the owner. Additionally, a dishonest cloud vendor U_P can disregard the model's integrity by compressing the model to save on storage. As a result, the actual model \hat{f} stored and deployed on the cloud platform may differ from the model f uploaded by the model owner. It is important for the model provider U_M and clients U_C who purchased the API to verify that the model \hat{f} is the same as f . Moreover, the platform would benefit from using a lightweight, low-cost tool for the regular verification of the model's integrity. For example, making five times forward inference is more practical than checking a large number of parameters or hashing at an intensive time granularity.

Verification is then performed using a small number of fingerprinting samples that indicate the changes in the behavior of the compromised model \hat{f} as compared to the original model f . *Clients* who buy the MLaaS service to make predictions would use a set of (encysted sample, label) pairs to verify the integrity of the deployed model using the response from its API service. During verification inference, the user obtains $\text{FM} = \{(s_i, r_i)\}_{i=1}^V$ from the secure server where the repository of model fingerprints reside, and then queries the API of the deployed model \hat{f} on $\{s_i\}_{i=1}^V$. The model is not intact when $\exists i \in \{1, \dots, V\}$ such that $\hat{f}(s_i) \neq r_i$.

Threat Model. There are three main service procedures during and after deployment: model transition between owner

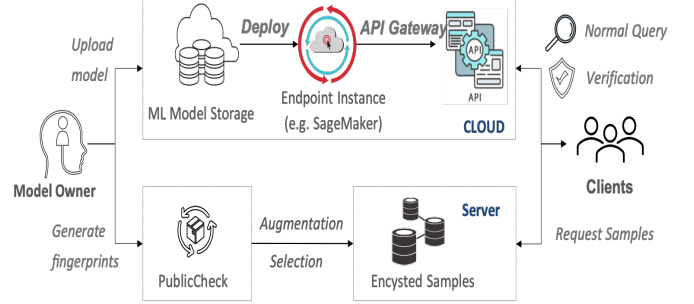


Figure 2: Structure of the PublicCheck watermarking.

and server, model storage in the cloud and inquiry service via API. After obtaining the fingerprints of the models using our PublicCheck, we assume the model's integrity could be compromised at any time, and no assumptions are made regarding how the model is modified, whether by an external attack or internal manipulation. (1) *Transmission Vulnerability*. The adversary can modify a model while it is transmitted from the *Model Owner* to the *Cloud* platform by exploiting vulnerabilities in cloud network protocols or service interfaces, i.e. during *Upload model* procedure in Figure 2. (2) *Storage Vulnerability*. Adversaries can exploit *ML Model Storage* vulnerabilities to substitute a compromised model for the safe one. (3) *Dishonest Cloud*. If the cloud vendor is dishonest, it may violate the SLA secretly for financial gains, such as compressing model data to save space without informing the customer.

The more problematic situation occurs with public verification when fingerprint samples are available to adversaries or if cloud providers compromise the integrity of the DNNs. We assume that the adversaries have white-box knowledge of the deployed models and fingerprinting samples. Furthermore, we evaluate the performance of our watermarking approach when faced with adaptive attacks in which an adversary is capable of collecting a large number of publicly available samples for all classes and then using those samples to prune/compress a model or introduce backdoors. Details are in Section 4.8.

Knowledge of Run-time Information for Fingerprinting Design. In the process of fingerprinting samples, even if the authorized user has all the model parameters and some of the training data, additional run-time information is also needed, such as gradient values. We refer to this situation as black-box access and white-box knowledge design. It is however difficult to obtain such run-time knowledge in many real-world applications, such as non-gradient optimization methods and protected gradient strategies (also known as black box knowledge). To generate a more generalized fingerprinting sample, we assume two knowledge settings concerning the run-time information used to construct the fingerprinting samples, black-box and gray-box knowledge. In general, the less knowledge of runtime information is available, the more generalized the fingerprinting approach will be.

Black-box Knowledge. The fingerprinting authenticator in black-box knowledge scenario has access only to a few training samples and the prediction service for the model to be verified, without access to any other knowledge about the target model, such as its parameters, structure and gradient information during fingerprinting design. This setting is common in real world applications. For example, the model obtained by the model owner is sometimes protected or encapsulated as executable files, such as binaries or executable files. Also, model files may be encrypted by compilation, shelling, or confusion, which makes them difficult to be decompiled. Because the gradient matrix or Hessian matrix cannot be obtained, stochastic gradient descent (SGD) cannot be used for optimizing deep learning models when the objective function cannot be precisely specified. In such situations, the black box algorithm are applied to determine the objective function. The common black box optimization methods include simulated annealing, the simplex method, and evolutionary strategies derived from evolutionary algorithms. In these scenarios, it is difficult to obtain the gradient information of the running model for the purpose of designing watermark samples. As a result, black-box assumptions must be made about the targeted models, especially for the gradient information.

Gray-box Knowledge. In the gray-box knowledge setting, the fingerprinting authenticator is assumed to have knowledge of part of training data and then train a substitutive model with respect to the target model, even with different structures and parameters.

3 PublicCheck System Design

To address the practicality, imperceptibility, and limited design knowledge challenges, we present a practical watermarking methodology with public verifiability based on encysted samples, named PublicCheck. As explained earlier, the intuition behind our model is that a minor manipulation in the model will manifest as a shift in the decision boundary, and the prediction around the decision boundary could be easy to be flipped, as shown in Figure 1. A slight change in the decision boundary indicates an integrity violation in the model. The model’s decision boundary could be used to generate its fingerprint for watermarking. There is a challenge in capturing the decision boundary with a limited number of available samples. The PublicCheck addresses this issue in the following manner. First, we augment a set of randomly sampled ordinary instances (called referenced samples) to become transformed variants densely around the decision boundary of the target model by using generative deep neural networks. We then select candidates that can capture the decision boundary using the inherent prediction behavior of the model according to the watermarking efficiency and naturality criteria. The overview of the scheme is illustrated in the Figure 3 and Algorithm 1.

Data Augmentation. We utilize attribute manipulation-based generation for efficient data augmentation, whereby

Algorithm 1: Public Verification of Model Integrity

Input: verification samples number v , target model f , maximum scale and variance of perturbation Δ_{max} , σ , endocer and decoder of pre-trained disentangled generative model En , De , max iteration I
Output: encysted samples for fingerprinting set ES and the verification result

```

1  $X_t \leftarrow$  Random samples from training datasets
2  $ES \leftarrow \{\}$ 
3 while  $|ES| < v$  do
4   for  $x$  in  $X_t$  do
5      $z \leftarrow En(x)$ 
6      $\mu \leftarrow argminf(De(z + \Delta z)) \neq f(De(z))$ 
7      $\Delta z \leq \Delta_{max}$ 
8     // Boundary value of noise
9      $\xi \leftarrow$  Adaptive Perceptual Similarity Threshold
10    // Section 3.4
11     $ES_x \leftarrow \{\}$ 
12    while  $i \leq I$  do
13       $\Delta z \sim \mathcal{N}(\mu, \sigma)$ 
14      if  $PS(De(z + \Delta z)) \geq \xi$  then
15        // Perceptual Similarity
16         $ES_x \leftarrow De(z + \Delta z)$ 
17       $i += 1$ 
18     $ES \leftarrow$  one random sample from  $ES_x$ 
19  Fingerprinting of  $f \leftarrow f(ES)$ 
20  Integrity of  $f' \leftarrow$  True if  $f'(ES) = f(ES)$  else False

```

data samples are augmented along a semantic feature axis. Variational autoencoder (VAE)-based generative models are developed to represent samples in the high-dimensional pixel space into a low-dimensional latent space via latent codes. Combined with disentanglement, they are capable of providing such a controllable mechanism. Our objective is to develop latent representations that encode distinct attributes of the data as separate latent codes. The disentangled latent representation indicates that changes in one part of a latent code correspond to changes in one attribute of data only, while remaining relatively invariant to changes in other attributes. We provide the **Generative Model with Disentanglement** at two levels of granularity: (a) attribute-level that indicates the change on the degree of the crook of a given handwritten digit) and (b) abstraction-level which illustrates the change of tiny texture on the human face in the Figure 4) disentanglement, as described in Section 3.1.

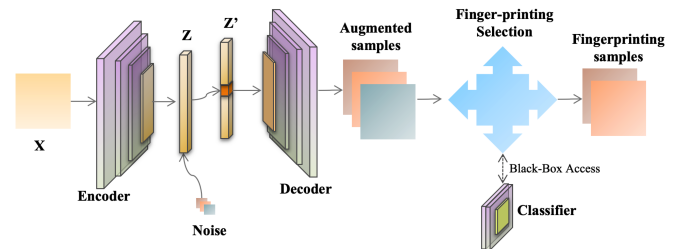


Figure 3: Overview of the PublicCheck watermarking

Control Augmentation. We next utilize a disentangled generative model, which has been pre-trained on clean data, to model the probability distribution of encysted samples from a given image and conduct data augmentation via latent perturbation to address the *Practicality*. Specifically, we first transform the clean data to its latent space representation (line 5 of Algorithm 1). Our next step is to identify the latent code that controls specific attributes. Then, using black-box inference of the target model, we add perturbations to the selected latent code until a change in the prediction of the reconstructed image is observed. We define the marginal value of the encysted boundary (e.g., μ) as the minimum perturbation value in the selected latent code that caused a prediction change (lines 6-7). Details are in Section 3.2 *Controllable augmentation and perturbation*.

Sample Selection. We then apply the *Selection of Encysted Samples for Fingerprinting* (lines 8-17, details in Section 3.3) to enhance the effectiveness and naturalness of the augmented encysted samples. The encysted sample inputs should make the model outputs the most sensitive to the decision boundary change regarding the encysted noise range. Therefore, even if the decision boundary is slightly modified, the prediction results of these encysted samples will almost certainly change. Consequently, we develop mechanisms to decide the μ with limited knowledge about the target model to address *Limited knowledge for design*, and define the encysted noise range σ to build a normal distribution $\mathcal{N}(\mu, \sigma)$. Then, the encysted samples are augmented from the original training instance via reconstructing the selected latent code after adding randomly sampled noise from the given distribution $\mathcal{N}(\mu, \sigma)$. In addition, encysted samples for fingerprinting are perceived to be natural to the human with the original inputs, and it is infeasible to recognize the fingerprinting patterns in the latent space from the pixel space. Therefore, we apply filtering strategies to select suitable encysted samples for fingerprinting to meet the naturalness criteria (address the *Imperceptible* concern) using an adaptive threshold to build a pool of natural samples for random selection. Finally, the the model’s fingerprint could be represented as a prediction vector for a small set of encysted samples for fingerprinting. During verification inference, the model is verified to be intact only when the response of the test model on the encysted sample set is equal to the fingerprint prediction vector (line 18-19). A visual illustration of our PublicCheck method provided in Figure 4.

3.1 Generative Model with Disentanglement

We introduce generative models with two levels of disentanglement in an unsupervised learning manner. These are attribute-level disentanglement based on low-dimensional latent representation vector and abstraction-level disentanglement based on high-dimensional latent representation.

As for relatively low-fidelity and simple images, such as

handwritten digits MNIST, the VAE-based generative model can be used to learn a simple representation of data in the latent space, e.g., a 20-dimensional latent code vector. In addition, attribute-level disentanglement can be attained by forcing the distribution of latent representations to be factorial via loss terms, leading to independent distributions across dimensions. An individual latent code reveals only a particular semantic attribute, such as one latent code that controls the thickness of the digits. To better balance the trade-offs between reconstruction quality and disentanglement, we adopt the Total Correlation [23] and adopt a human perceptual evaluation Learned Perceptual Image Patch Similarity (LPIPS) [52] as reconstruction error. Details are attached in Appendix A.1. The loss of VAE incorporated with a TC term is given as follows:

$$\mathcal{L}_{VAE} = \mathcal{L}_{Rec} - D_{KL}(q_{\phi}(z|x) || p(z)) - \nu TC(z) \quad (1)$$

The first term \mathcal{L}_{Rec} is the reconstruction error based on LPIPS, which assesses whether the latent codes z is informative enough to reassemble the original instance. The second part is a regularization term, to push Encoder $q_{\phi}(z|x)$ to match the prior distribution $p(z)$, e.g., a Gaussian distribution. The third part is the TC term, to measure the dependence for multiple random variables. The ν is set at 40.

For high-fidelity and complicated images, such as high-resolution human face images, or multi-domain images such as CIFAR-100, the dimension of the latent codes should be largely extended to maintain more features. Therefore, the disentanglement strategies used for disentangle-VAE are not applicable. Accordingly, we provide an abstraction-level disentanglement strategy to handle high-fidelity and complicated images. We extend the scale of the latent codes and divide them into a style (high abstraction) level and a texture (low abstraction) level latent representation, via two separate encoders. To extend the latent representation, we apply the Vector Quantized strategy used in [37, 41]. In general, VQ-based autoencoders consist of three components, encoder En , decoder De , and codebook C . The codebook C can be viewed as a common feature dictionary shared between the encoder and decoder, consisting of K categorical embedding items with D dimensions. The encoder is a non-linear mapping from the input instance x in the pixel space to the latent representation $z_e(x)$, consisting of latent embedding vectors with D dimensions. Vector Quantization is to map $z_e(x)$ to a discrete latent matrix with each element representing the index of the nearest embedding items in the codebook for each latent embedding vector of $z_e(x)$. The decoder reconstructs back to pixel space using the queried embedding items $z_q(z)$ corresponding to the discrete latent index matrix via another non-linear function, as shown in Figure 5. Details of VQ based generative model are in Appendix A.2.

To achieve abstraction-level disentanglement, we apply two separate (encoder, codebook) pairs to model texture information and style information, respectively. A global encoder En^g

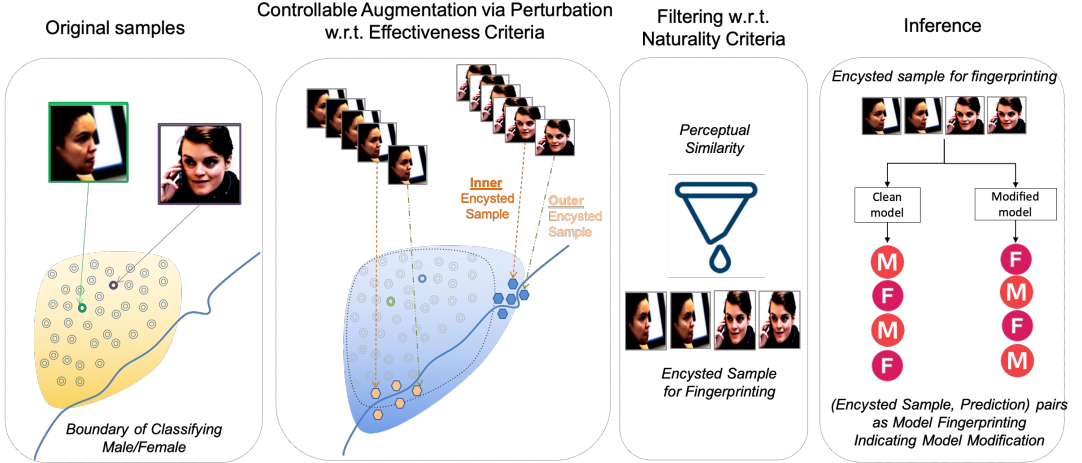


Figure 4: Visual illustration of our public watermarking.

and codebook C^g is applied to capture high-abstractive information, such as style, shape, and geometry, and a local encoder En^l and codebook C^l is used to capture low-abstractive information, such as texture, color or background. Specifically, the local encoder initially maps the input instance into local latent representation $z_e^l(x)$ using En^l , followed by conducting global encoder En^g to map $z_e^l(x)$ into $z_e^g(x)$. Then we transfer the $z_e^g(x)$ into a discrete latent matrix z^g via vector quantization by nearest neighbor searching on the global codebook C^g . The global decoder De^g is then applied to recover the latent representation back to a representation s^l with the same size as $z_e^l(x)$. The composed $\hat{z}_e^l(x) = s^l + z_e^l(x)$ are vector quantized into a discrete latent matrix z^l via nearest neighbor searching on the local codebook C^l . Finally, the local decoder De^l takes as input all levels of the quantized latent representation back to the original image size. Here, we also replace the default pixel-wise reconstruction evaluation with the perceptual evaluation metric LPIPS. The generative models are assumed to be trained on the part of the training data of the target model or the similar public-available datasets.

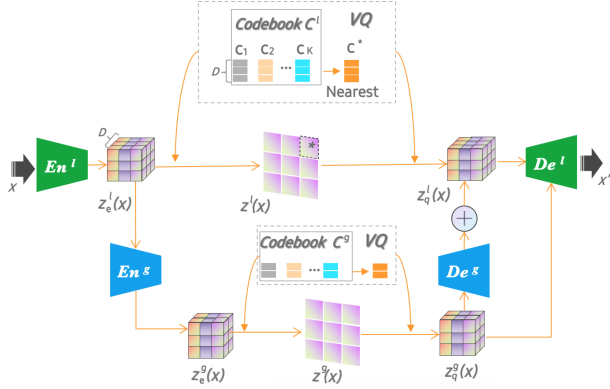


Figure 5: Demonstration of VQ-based generative model.

3.2 Controllable Augmentation & Perturbation

The decision boundary of a model is its inherent and direct fingerprinting on the training data. Therefore, we aim to conduct data augmentation around the decision boundary of the target model, through the use of generative deep neural networks on a limited number of available reference samples.

We apply an attribute manipulation-based generation to enable controllable augmentation, whereby data samples are augmented along a semantic feature direction via adding perturbation into the latent space. Based on the disentangled latent representation derived from the *Generative Model with Disentanglement*, encysted sample augmentation is conducted via adding certain perturbation Δz into specific latent codes that clearly control a semantic attribute, followed by reconstructed to the pixel space via decoder $De(z + \Delta z)$. The perturbation will be added to the selected elements of the latent code vector as attribute-level disentanglement, or the entire low abstraction latent representation as abstraction-level disentanglement.

Encysted samples are defined as reconstructed copies from perturbed latent representations, where noise is from a given distribution within a given scale (e.g., normal distribution $\mathcal{N}(\mu, \sigma)$). Given a target model $f(x)$, we define the marginal value of the encysted boundary (e.g., μ) as the minimum value that changes the prediction (i.e., $\text{argmax}_{\Delta Z} f(De(Z + \Delta Z)) \neq f(De(Z))$), detailed in Section 3.3. Scale σ defines the encysted noise range with the maximum noise scale (upper bound $\mu + \sigma$) and the minimum scale (lower bound $\mu - \sigma$). Encysted samples $ES = \{es_1, \dots, es_n\}$ are defined as reconstructed copies using the perturbation sampled from normal distribution $\mathcal{N}(\mu, \sigma)$. Within the encysted noise range, the predictions of the reconstructed encysted samples using the perturbed latent codes are easy to be flipped. An encysted sample derived from x that produces a changed prediction is

referred to as the outer encysted sample, and vice versa, the inner encysted sample. Depending on the randomly sampled noise, reconstructed encysted samples are either the inner or outer samples.

3.3 Selection of Encysted Samples

To meet the effectiveness criteria of fingerprinting sample selection, we develop two strategies to effectively select the encysted noise distribution $\mathcal{N}(\mu, \sigma)$ for the generation of the encysted sample, under limitation of the knowledge about the target model to be verified. The next step is to apply the filtering strategy to select suitable encysted samples for fingerprinting to meet the naturality criteria.

3.3.1 Black-box Knowledge for Fingerprinting Design

To address the black-box knowledge setting of fingerprinting authenticator in Section 2, we conduct the black-box knowledge fingerprinting design as follows. This case aims to determine the outer bound of noise, namely, the minimum noise scale added to the latent representation that changes the prediction of the corresponding reconstructed image. Formally, the perturbation of the latent representation can be considered as the optimization of ΔZ using the Carlini and Wagner (C&W) loss:

$$\mathcal{L}(De(Z + \Delta Z)) = \max(0, \log f(De(Z + \Delta Z))_y - \max_{c \neq y} \log f(De(Z + \Delta Z))_c) \quad (2)$$

Here, Z is the latent codes for input x , the $f(\cdot)_y$ reveals that the output of the function f is y . The minimum loss is achieved when $f(De(Z + \Delta Z))_y \leq \max_{c \neq y} f(De(Z + \Delta Z))_c$, namely, we reach the outer bound of the noise ΔZ . Thus, finding the outer bound of latent perturbation for the input data x can be defined as follows:

$$\Delta Z_{outb} = \arg \min_{\Delta Z \leq \Delta_{max}} \mathcal{L}(De(Z + \Delta Z)) \quad (3)$$

Here, Δ_{max} is condition to terminate the perturbation searching.

In the BlackBox knowledge case, Eq. 3 is optimized via only accessing the inputs and outputs of the function f (e.g., a classifier). Therefore, the Natural Evolution Strategies (NES) is adopted to optimize Eq. 3 via search gradients. We define the latent noise ΔZ to be from an isometric normal distribution with mean μ and standard deviation σ , denoted by $\mathcal{N}(\Delta Z | \mu, \sigma^2 I)$. Then we use parameters \mathbf{t} as $\{\mu, \sigma\}$ [9, 27, 49]. NES defines a search distribution $p(\cdot | \mathbf{t})$ on $\mathcal{L}(\cdot)$, $De(Z + \Delta Z)$ is denoted by \cdot to simplify notation, followed by optimization under this distribution using the following objective:

$$J(\mathbf{t}) = \mathbb{E}_{p(\cdot | \mathbf{t})} [\mathcal{L}(\cdot)] = \mathbb{E}_{\mathcal{N}(\Delta Z | \mu, \sigma^2 I)} [\mathcal{L}(De(Z + \Delta Z))] \quad (4)$$

Gradient descent is then used to optimize the Eq. 4 by figuring out the Jacobian of $J(\mathbf{t})$. Here, σ is considered as

a hyperparameter and the loss $J(\cdot)$ will be only optimized with respect to μ . The parameters \mathbf{t} will be updated via a gradient descent step with a learning rate α as follows:

$$\begin{aligned} \mathbf{t}_\mu &\leftarrow \mathbf{t}_\mu - \alpha \nabla_{\mu} J(\mu, \sigma), \\ \nabla_{\mu} J(\mu, \sigma) &= \mathbb{E}_{\mathcal{N}(\Delta Z | \mu, \sigma^2 I)} [\mathcal{L}(\cdot) \nabla_{\mu} \log(\mathcal{N}(\Delta Z | \mu, \sigma^2 I))] \end{aligned} \quad (5)$$

Finally, we generate the encysted samples by reconstructing the perturbed latent representation using the noise ΔZ sampled from $\mathcal{N}(\Delta Z | \mu, \sigma^2 I)$.

3.3.2 Gray-box Knowledge for Fingerprinting Design

To address the gray-box knowledge setting of fingerprinting authenticator in Section 2, we conduct the gray-box knowledge fingerprinting design as follows. This case aims to obtain approximation for the outer bound of noise using the given pair of substitutive model \mathcal{M} for the target model f and its attacked version \mathcal{M}° . Namely, the minimum noise scale added to the latent representation distinguishes the prediction of \mathcal{M} from that of \mathcal{M}° on the same reconstructed image. Formally, the perturbation of the latent representation can be considered as the approximation of ΔZ using the loss:

$$\mathcal{L}(De(Z + \Delta Z)) = \max \left(0, \log \mathcal{M}(De(Z + \Delta Z))_y - \max_{c \neq y} \log \mathcal{M}^\circ(De(Z + \Delta Z))_c \right) \quad (6)$$

The minimum loss is achieved when $\mathcal{M}(De(Z + \Delta Z))_y \leq \max_{c \neq y} \mathcal{M}^\circ(De(Z + \Delta Z))_c$, namely, we reach one approximation of as outer bound of the noise ΔZ . Finding the outer bound of latent perturbation for the input data x is defined as:

$$\Delta Z_{outb} = \arg \min_{\Delta Z \leq \Delta_{max}, \mathcal{M}(De(Z + \Delta Z)) = \mathcal{M}(De(Z))} \mathcal{L}(De(Z + \Delta Z)) \quad (7)$$

We define the latent noise ΔZ from an isometric normal distribution with mean μ and standard deviation σ , denoted by $\mathcal{N}(\Delta Z | \mu, \sigma^2 I)$. In this case, we directly use the approximation of ΔZ_{outb}^x as the μ^x for each input x , while σ is considered as a hyperparameter. Finally, we generate the encysted samples by reconstructing the perturbed latent representation using the noise ΔZ sampled from $\mathcal{N}(\Delta Z | \mu, \sigma^2 I)$, targeting function f .

3.3.3 Filtering via Adaptive Similarity

Following augmentation of the encysted samples using perturbation scales derived from the two strategies above, the next step is to use the filtering strategies to select suitable encysted samples to be fingerprinted to meet the naturality criterion. We retain only the encysted samples that have a higher similarity evaluation based on LPIPS. A fixed threshold for perceptual similarity is difficult to establish for different data types, so we propose an adaptive approach for assessing naturality. Given a small set of reference instances (generally around 10) randomly selected for each class, denoted by RI_c , the LPIPS loss metric is then applied to calculate the similarity between every two instances of the same class. We use the

average similarity as the adaptive threshold ξ_c of each class for the filtering. During the filtering, given a reconstructed encysted sample candidate es_i , the adaptive threshold ξ_c and reference instance set RI_c according to its predicted class via $f(es_i) = c$ are used to decide the filtering results. Specifically, we calculate the LPIPS similarity between the es_i and each sample in RI_c . The encysted sample es_i will be selected as fingerprinting sample only if all distances are smaller than the threshold ξ_c . Formally, the encysted sample for fingerprinting is satisfied only when $LPIPS(es_i, ri) \leq \xi_c, \forall ri \in RI_c$.

4 Evaluations

The performance of PublicCheck is evaluated on three datasets: MNIST [26], CIFAR-10 and CIFAR-100 (274 × 274) [24], and FFHQ (1024×1024 human face) [21, 22]. The target classifiers for these three datasets are adopted the LeNet, ResNet-18 [18], and VGG-16 [43], respectively. Appendix B shows the details of the datasets and classification models used in our experiments, as well as the corresponding accuracy without having any attacks. Note that 20% of the dataset will be randomly separated as additional data (i.e., as the public-available relevant datasets) for the generative model training. A small set of instances (normally less than 20) are randomly sampled from the remaining 80% as the reference samples for augmentation, watermarking design and evaluation. The number of reference samples is generally 3-4 times of required number of the encysted sample for fingerprinting. The VAE-based generative model (attribute-level disentanglement) is used for MNIST, and VQ-based generative model (abstraction-level disentanglement) is used for CIFAR and FFHQ. Detailed architecture and hyperparameters are given in Appendix C.

4.1 Evaluation Goals and Metrics

An evaluation’s first objective is to determine the detection success of integrity breaches under various attacks and model compression. In general, the less information derived from the underlying target model, the more difficult it is to verify integrity. Therefore, we assume the worst-case scenario of API access, where only the Top-1 classification label can be obtained. Specifically, the API will only return the most likely label for a query, instead of a list of top k results. The fingerprinting of the model is represented as the Top-1 classification prediction of the original model on a set of encysted samples for fingerprinting, denoted by (ES, Y) , which is conducted by the model owner. For a given a set of fingerprinting pairs $\{(es_1, y_1), (es_2, y_2), \dots, (es_M, y_M)\} \subset (ES, Y)$ and the predictions of these given encysted samples through the black-box access to evaluated model, $\hat{Y} = \{\hat{y}_1, \hat{y}_2, \dots, \hat{y}_M\}$, we define the detection success rate of integrity breach as: $\exists \hat{y}_i \in \hat{Y}, \hat{y}_i \neq y_i$. We report the detection success under both black-box and gray-box knowledge cases in Section 4.3. We also investigate

the performance of our PublicCheck under more restricted scenarios in Section 4.4, in which the availability of reference samples is limited. In addition, we evaluate the overheads associated with designing and implementing fingerprinting samples in Section 4.5. Additionally, we also evaluate the performance of our method when varying the hyperparameters, such as noise scale, in Section 4.6. Furthermore, we evaluate the naturality of the encysted sample for fingerprinting in Section 4.7. We compare our approach to the baseline (randomly selected original reference samples) and the *Sensitive Sample* [19] for the private verification of model integrity. Note that we allow white-box knowledge on target models for Sensitive Sample design.

4.2 Experimental Setups

We mimic two adversarial settings of the integrity breach in the experiments. *Adversarial attacks* that compromised the model during model transition or storage in the cloud, assuming that the target model is known and under the attacker’s control. *Dishonest cloud vendors* that conduct model compression to save storage space.

(1) For the *adversarial attacks*, we deploy three attacks with the TrojanZoo [38] platform, including the BadNet [16], TrojanNN [50], and CleanLabel [44] attacks on the image classification models, as the typical poisoning attacks that compromise the training data to change the model’s behavior at test time. We assume the attacker attempts to maximize the degradation of prediction accuracy of the actual class as well as the possibility of being misclassified as a target class. A Trojan model typically reacts to trigger-embedded inputs with such malicious functions, but otherwise behaves normally. Backdoor attacks infect target systems with more slight changes of parameters than misclassifying to the target class. The misclassifying attack success rate of each of these three adversarial models was more than 95%. The default settings of these attacks are in Appendix E.

(2) For the *dishonest cloud vendors*, we apply weight pruning to compress the models on three datasets. Pruning starts by learning the connectivity via regular network training. Next, all connections with weights below a threshold are removed, followed by retraining the network to learn the final weights for the remaining sparse connections. The network is pruned by retaining only important connections, with around 15% of weights removed for the LeNet model on the MNIST dataset, 20% removed for the ResNet model on the CIFAR-10 dataset, and around 24% removed for the VGG16 model on the FFHQ dataset. Pruning hardly resulted in a change in the accuracy of (< 2%) for each model.

4.3 Evaluation on Integrity Breach Detection

4.3.1 Black-box Knowledge Setting Evaluation

Under this setting, the design of the encysted sample for fingerprinting is based on the encysted noise range only using the μ and user-specific scale σ in Section 3.3.1. The default perturbation scale is 0.05.

The results of the detection success rate against three attacks are reported in Figure 6. As shown, the success detection rate rises when increasing the number of encysted samples for fingerprinting from 1 to 10. Using only two encysted samples for fingerprinting, the detection rate of the integrity breach could achieve more than 93% for MNIST (97.9% for CIFAR-10, and almost 100% for FFHQ) against all three testing attacks, compared to below 10-20% for the *randomly selected training samples*. It demonstrates that the detection rate increases when the target model grows to be huge and complex. The reason is that the complex model has a more complicated decision boundary, and our method has more sources to design the fingerprinting. With five encysted samples for fingerprinting, our method achieves 100% detection accuracy for all testing datasets under all testing attacks. The overhead of model integrity validation is minimal at the cost of only five API queries.

To evaluate the effectiveness of our watermarking approach on a dataset of a larger class number, we also used the CIFAR-100 dataset. As shown in Figure 7, using only one encysted sample for fingerprinting, the detection rate of the integrity breach could achieve more than 88% for CIFAR-100 against all three testing attacks, as opposed to 76% for CIFAR-10. In terms of CIFAR-100, two encysted samples could increase the detection accuracy to 98% and four samples to 100%. As a result of the more complex decision hyperplane, the detection rate increases when the classification task has more classes.

In addition to the above 3 attacks, we also evaluate the successful detection rate of model integrity breaches caused by model compression, as shown in Figure 7. Using only two encysted samples for fingerprinting, the detection rate of the integrity breach for our method could achieve around 97% for MNIST and CIFAR 100 (98.0% for CIFAR-10 and FFHQ, 98.6% for CIFAR-100) against the compressed model (with 15-25% parameters removed), compared to below 10-15% for the randomly selected training samples. Additionally, the detection rate increases when more complex models are verified. Using five encysted samples to fingerprint the model, we achieve 100% detection accuracy for all test datasets against the model compression, demonstrating the minimal overhead associated with verification. For the dataset with a larger class number, e.g., CIFAR-100, using only one encysted sample for fingerprinting, the detection rate of the integrity breach could reach more than 90% for CIFAR-100 against model compression, compared to 57% for CIFAR-10. Four encysted samples of CIFAR-100 are able to achieve 100% detection accuracy. This also confirms the effectiveness of our water-

marking approach when applied to a dataset with a greater number of classes.

Comparison with SOTA. We select the *Sensitive Sample* [19] as the state of the art (SOTA) for the private verification of model integrity. For the attacked model detection, the performance of our PublicCheck is similar to that of Sensitive Sample. Intuitively, the change of parameters under model compression is more significant than attacks, as a large fraction of parameters is removed with values reduced to zero instead of slightly modified. Therefore, the detection rate for model compression is anticipated to be higher than the integrity verification under attacks, as demonstrated in our results. We compare the performance of PublicCheck with sensitive samples from [19], taking the classifier of CIFAR-10 under the same model compression settings as an example. Using only two samples, our approach could achieve a 98.0% detection rate for the CIFAR-10 dataset, compared to below 10% for the randomly selected training samples and around 84.4% for sensitive samples. Five samples are sufficient to achieve 100% detection for our method. In contrast, 10 samples are not enough to achieve 100% detection rate for the sensitive sample approach.

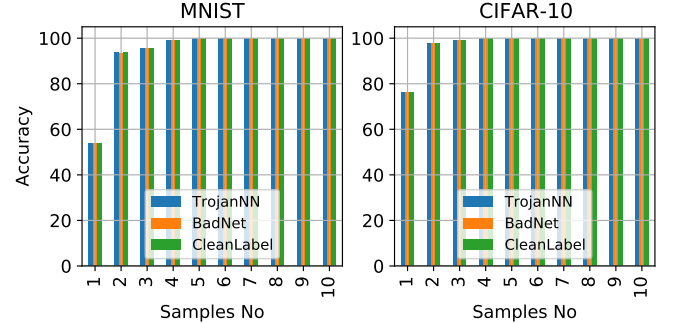


Figure 6: Success detection rate for model integrity breaches under three attacks (TrojanNN, BadNet, and Clean-Label) under black-box knowledge setting. The axes are the number of encysted samples for fingerprinting and the detection rate (%).

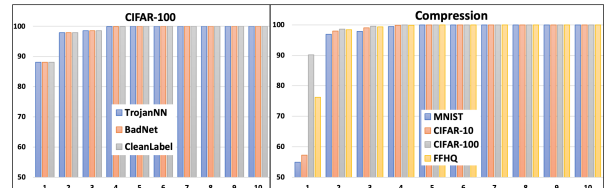


Figure 7: Success detection rate for model integrity breaches (a) under three attacks for CIFAR100 and (b) under model compression on MNIST, CIFAR-10, CIFAR-100 and FFHQ datasets under black-box knowledge setting. The axes are the number of encysted samples for fingerprinting and the detection rate.

It is interesting to note that the performance of sensitive samples for model compression is much worse than attacks. This has demonstrated the major limitation of the sensitive sample and another adversarial example alike approach under the public verification of model integrity scenario. The reason is that the design of the adversarial perturbation used to reveal

the changes in parameters of the target model is based on the activation or gradient of parameters’ updates during training. At the same time, the model compression approaches such as pruning also utilize similar signals to remove parameters with lower activation, resulting in degradation of detection of the model change. Due to this, the gradient-based perturbation for fingerprinting was not able to detect the model changes caused by attacks or compression approaches that utilize similar gradient information. These results indicate that our PublicCheck can achieve state-of-the-art performance for model integrity verification against diverse attacks and model compression under the black-box knowledge settings. The advantage of our approach is that a high detection accuracy can be achieved without requiring any knowledge of model parameters or structure and with a lower cost associated with designing fingerprint samples—only forward procedures are required.

4.3.2 Gray-box Knowledge Setting Evaluation

Here, we evaluate the PublicCheck under the gray-box setting where more information about the model is available. Under this setting, the design of the encysted sample for fingerprinting is based on the substitutive model of the target model and its attacked versions (Section 3.3.2). As shown in Figure 8, we again see that the success detection rate rises when increasing the number of encysted samples for fingerprinting. Using only one encysted sample for fingerprinting, the detection rate of the integrity breach grows by above 22% than the black-box knowledge setting for MNIST (by 11% than CIFAR-10) against adversarial attacks. There are also improvements (around 1%) for remaining testing settings of the encysted sample number until achieving 100% detection accuracy using five encysted samples for fingerprinting, for all testing datasets under all testing attacks. Additionally, we also evaluate the successful detection rate of model integrity breaches caused by model compression under the gray-box knowledge setting. Using only one encysted sample for fingerprinting, the detection rate of the integrity breach could increase by 15 – 20% for these testing datasets compared to that under black-box knowledge setting.

Our results indicate that our PublicCheck can perform better against diverse attacks and model compression under gray-box knowledge settings compared to black-box knowledge settings, randomly selected training samples, and sensitive samples, particularly for the model compression cases. The results demonstrate that the detection rate increases with more information about the target model when substitute models are available. As five encysted samples for fingerprinting can obtain the 100% accuracy of model integrity verification for both black-box and gray-box knowledge settings, the former seems to be the more reasonable choice due to no assumption on the model itself. These results also demonstrate the advantage of our PublicCheck in terms of *practicality* and

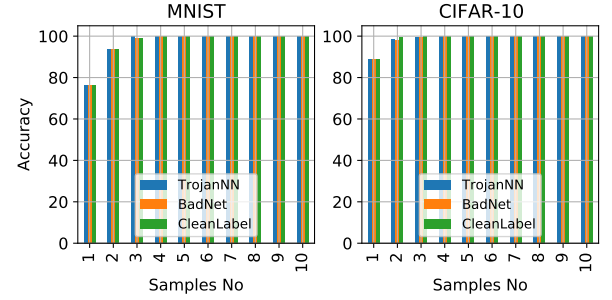


Figure 8: Success detection rate for model integrity breaches under three attacks (TrojanNN, BadNet, and Clean-Label) under gray-box knowledge setting. The axes are the number of encysted samples for fingerprinting and the detection rate (%).

performance under *under limited knowledge*.

4.4 Performance under Restricted Setups

In this part, we examine the performance under more restrictive circumstances. In particular, more restrictive assumptions are made regarding the limited categories of reference samples used to generate encysted samples for fingerprinting and the limited number of overheads associated with queries. Our default assumption for the black-box knowledge settings (used in the previous section) is a set of training data as reference samples covering most of the classes to design the encysted samples for fingerprinting. However, the available training samples may not encompass all classes of the entire dataset. Specifically, we examine this more limited setting, in which a small set of reference samples covering only a few categories may be used. This is a more practical application scenario. In the following, we report our investigation on the impact of the limited categories on integrity violation detection accuracy. We compare the performance of PublicCheck in detecting attacked models on MNIST and CIFAR-10 when encysted samples are generated by using only a subset of classes, e.g., by randomly sampling 1, 2, 3, or 5 of the classes, instead of using all ten classes in each dataset.

Next, we evaluate whether the detection rate of model integrity breaches could be 100% within the limited number of API queries. Results are averaged over these two datasets and all 3 TrojanZoo attacks. We report the results in Table 1. In general, we observe an increase in accuracy as the number of classes increases. Although the detection rate of our PublicCheck under 1, 2, 3, or 5 classes restriction has a slight drop compared to all-classes available scenario, it is demonstrated that even when watermark samples are created for one class only, PublicCheck still achieves 100% accuracy when using seven watermark samples for verification. It shows that five samples are enough to achieve 100% detection accuracy using PublicCheck, assuming the reference samples used to generate encysted samples for fingerprinting are only available for randomly selected five classes. Furthermore, the variances

of detection accuracy against different attacks decrease as the number of encysted samples increases. Additionally, the variances of detection accuracy are similar across classes.

It demonstrates our approach’s generalization ability, relying on the well-encysted and fine-granularity measure of the decision boundary using the attributed augmentation in the latent space. Specifically, due to the nature of PublicCheck, each encysted sample is generated from a randomly sampled perturbation, which lies very close to a random part of the decision boundary of the classification model. The prediction on the encysted sample for fingerprinting is used to distinguish whether the boundary of the verified model has the right disturbed in that localized region. Every additional watermarking sample then may test a different localized region of the decision boundary, thereby increasing the detection ability of PublicCheck.

4.5 Performance When Varying Noise Scale

To conduct the augmentation, we add a perturbation to the latent code that controls specific attributes. Generally, the generation of encysted samples aims to produce inner and outer encysted samples as close to the decision boundary as possible, via reconstructing the selected latent code after adding randomly sampled noise from the given distribution $\mathcal{N}(\mu, \sigma)$ under the black-box knowledge settings. As the noise scale σ should be decided in advance as a hyperparameter, we now demonstrate *“How scaling the noise impacts the accuracy?”*. Intuitively, a smaller noise scale σ , could result in a better performance of the fingerprinting samples since smaller noise leads to inner and outer samples being closer to the decision boundary. We conduct experiments to evaluate the detection rate of our method when varying the noise scale σ . The results are reported in Table 2, confirming the intuition above that a smaller noise scale brings a higher detection rate. Even under the broader noise scale, i.e., 0.1 or 0.5, six or nine encysted samples for fingerprinting are sufficient to achieve 100% detection accuracy, demonstrating the effectiveness of our method with the flexible settings. Furthermore, the variances of detection accuracy against different attacks decrease as the number of encysted samples increases. Furthermore, the variances of detection accuracy are also reduced as the scale of noise decreases. Generally, there is a trade-off between accuracy and overheads of computation. If smaller steps are taken, it takes more iterations to find the marginal value of the encysted boundary (e.g., μ). Accordingly, a broader noise scale could improve the performance of a fast and flexible fingerprinting design, which is suitable for resource-constrained devices. We demonstrate this argument in the next section with respect to the runtime overheads.

4.6 Overheads for Fingerprints Design

During public verification, a large number of fingerprinting samples will be produced with limited overhead, e.g., within a short period of time. We examine the run time as an overhead measure to demonstrate the practicality of PublicCheck. We mimic the end-users as a laptop with GPU resources (NVIDIA Quadro RTX 4000 8GB and i7 9900 16G CPU), and the other has CPU resources only (i5 8265U 8GB CPU).

Two types of consumed time will be examined. One is the generation of one individual encysted sample and the other is the generation and selection of one natural encysted sample (which we refer to as generation of one natural encysted sample). The run time to generate a single encysted sample for fingerprinting for three given datasets under various noise scale settings is reported in Table 3. Given the once-off trained generator, the encysted noise range, and the default noise level 0.05 used in our experiments, the generation time of each encysted augmentation is less than 2s for all testing datasets, including the high-fidelity images such as FFHQ images. For MNIST and CIFAR datasets, the time are 0.33s and 0.83s for each encysted augmentation, respectively. We also report the generation time for each augmentation of high-fidelity FFHQ images for CPU-Only end user, which is around 15s per augmentation.

To ensure the natural requirement under public verification, a further filtering procedure is conducted on the set of augmented encysted samples. The overhead for the filtering procedure is minimal, less than 0.2s for selecting one natural encysted sample for fingerprinting. The total time for the combination of augmentation and filtering of one encysted sample for fingerprinting varies from roughly 2 seconds for MNIST, CIFAR-10 and CIFAR-100, to roughly 9 seconds for FFHQ, under 0.05 noise level for GPU end users. For CPU-only users, runtime is similar to GPU users’ for simple cases like MINIST and CIFAR-10 but can be longer for tasks involving larger class numbers or high fidelity inputs. A possible solution for CPU users is to perform parallel processing for LPIPS evaluation across classes and generation of encysted samples. Once watermarking samples have been generated, the time required to verify a deployed model is less than 0.2 s per sample. Therefore, we can expect model verification to take less than one second when we have five watermarking samples. Thus, our solution can be deployed in real-time applications.

There is a trade-off between noise scale and overheads of computation. The broader the noise scales, the less time used to conduct the encysted samples for fingerprinting. To achieve more efficient verification, smaller noise scales must be used, which means more iterations are needed to determine the marginal value of the encysted boundary. As demonstrated in Section 4.5, even under the larger noise scale, i.e., 0.5, nine encysted samples for fingerprinting are sufficient to achieve 100% detection accuracy, demonstrating the effectiveness

Table 1: Impact on detection rate (%) of increasing the number of classes with encysted samples. The row is the number of classes of reference samples with generated encysted samples and the column is the number of encysted samples for verification. As the performances are very similar for both MNIST and CIFAR-10, we report the results and variances for combining them as a generalized case study.

Classes #	1	2	3	4	5	6	7	8	9	10
1	59.0 \pm 8.2	92.1 \pm 2.3	94.1 \pm 2.1	97.8 \pm 0.4	99.2 \pm 0.3	99.8 \pm 0.1	100 \pm 0	100 \pm 0	100 \pm 0	100 \pm 0
2	59.0 \pm 8.2	94.4 \pm 2.0	94.8 \pm 1.9	98.1 \pm 0.4	99.8 \pm 0.1	100 \pm 0.0	100 \pm 0	100 \pm 0	100 \pm 0	100 \pm 0
3	59.0 \pm 8.2	94.6 \pm 1.9	96.7 \pm 0.5	99.1 \pm 0.3	99.9 \pm 0.1	100 \pm 0.0	100 \pm 0	100 \pm 0	100 \pm 0	100 \pm 0
5	59.0 \pm 8.2	94.8 \pm 1.9	96.8 \pm 0.5	99.3 \pm 0.2	100 \pm 0	100 \pm 0	100 \pm 0	100 \pm 0	100 \pm 0	100 \pm 0

Table 2: Impact on detection rate (%) of increasing the range of noise scale σ . Row is the scale of noise to guide the generation of encysted samples for fingerprinting, column is the number of fingerprinting samples for verification. Also, the generalized results and variances on MNIST, CIFAR-10 and FFHQ are reported.

Noise	1	2	3	4	5	6	7	8	9	10
0.01	65.1 \pm 7.2	95.7 \pm 1.2	97.9 \pm 0.4	99.9 \pm 0.1	100 \pm 0	100 \pm 0	100 \pm 0	100 \pm 0	100 \pm 0	100 \pm 0
0.05	59.0 \pm 8.0	94.9 \pm 1.8	96.8 \pm 0.5	99.4 \pm 0.2	100 \pm 0	100 \pm 0	100 \pm 0	100 \pm 0	100 \pm 0	100 \pm 0
0.1	44.5 \pm 9.2	87.9 \pm 3.1	90.4 \pm 2.5	93.6 \pm 2.1	95.5 \pm 1.2	99.5 \pm 0.2	100 \pm 0	100 \pm 0	100 \pm 0	100 \pm 0
0.5	30.3 \pm 9.9	53.4 \pm 8.2	66.4 \pm 7.5	79.8 \pm 5.4	84.3 \pm 3.9	92.4 \pm 2.3	95.7 \pm 1.1	98.7 \pm 0.3	100 \pm 0	100 \pm 0

of our method with the flexible settings. In this setting, the generation of the encysted samples for fingerprinting with naturality filtering takes around 1 second for all three datasets, including high-fidelity images.

Comparison with SOTA. We select the *Sensitive Sample* [19] as the SOTA for the private verification of model integrity. By comparison, we also tested the time to generate sensitive samples on the same dataset, taking human face images as an example under the GPU settings. It took 2964.5s to generate 100 samples, and then an additional 725 seconds to select the best 10 examples from those 100 according to its Maximum Active-Neuron Cover Sample Selection, giving a total time of 3689.5 seconds to generate 10 samples. Using a filtering ratio of selecting the 10 best samples from a pool of 100 generated samples, the time to generate a single watermark sample is roughly 369 seconds, compared to around 1s for our PublicCheck. Reducing this filtering procedure would reduce the generation time at the cost of degradation of the performance for the selected sensitive samples. However, since the time to generate one candidate sensitive sample (with no filtering) is still of the order of 29.6 seconds, revealing that the generation of PublicCheck is still a lot faster.

Table 3: Time (s) required to generate a natural watermarking sample for various noise levels under GPU/CPU settings.

Dataset	0.5	0.1	0.05	0.01
MNIST	0.5 / 1.34	1.2 / 2.01	2.3 / 2.28	7.1 / 20.1
CIFAR-10	0.6 / 0.74	1.33 / 1.51	2.07 / 2.88	7.8 / 13.3
FFHQ	1.2 / 15	4.8 / 25	9.1 / 59	44.4 / 230

4.7 Naturality Evaluation

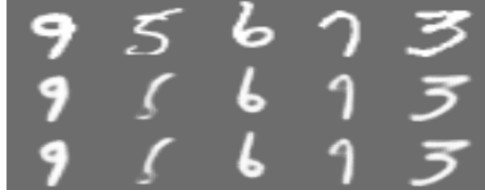
We demonstrate the naturality of the generated encysted sample for fingerprinting in this section. We first visualize the produced encysted samples for fingerprinting in Figure 9. As shown, there are few artifacts introduced in the encysted samples compared to the original reference samples. Generally, the generated samples' small texture or color temperature is modified via manipulating the corresponding latent codes. Thus, from human perception, these generated encysted sam-

ples are similar to the natural ones. These results confirm the advantages of our method under the public verification scenarios. In addition to this, we also report the quantitative evaluation of the naturality of encysted samples for fingerprinting, using the LPIPS metric in Figure 10. The average LPIPS values of the encysted samples for MNIST and CIFAR-10 among classes are approximately 0.2, and 0.45 and 0.55 for CIFAR-100 and FFHQ, respectively. The naturality of encysted samples for fingerprinting are obvious and consistent among different classes for all these three datasets (FFHQ is a male and female class), demonstrating that they are natural for human perception.

Comparison with SOTA. For the randomly augmented encysted samples, around 25% of them satisfies the naturality evaluation in terms of the adaptive threshold (0.57). In contrast, our experiments demonstrate that only 1% of sensitive samples meet the adaptive naturality threshold (LPIPS=0.65). Considering the time cost, generating one natural sensitive sample takes more than 3600s (1h), which is infeasible in practice. Our PublicCheck only takes 9 seconds to generate one natural encysted sample for fingerprinting. Besides, the visualisation of the successful sensitive samples is given in the Appedix D, which does not seem natural for human perception despite having small pixel-wise error.

4.8 Adaptive Attack Evaluation

Since encysted samples are visible to the public, including adversaries, we also evaluate the performance of our watermarking approach when faced with adaptive attacks. This setting assumes that an extreme adversary is capable of collecting a large number of publicly available encysted samples for all classes and then using these samples to prune/compress a model or introduce backdoors. Adaptive attacks are similar to adversarial training based defence strategies. Specifically, for a given dataset (CIFAR-10 or MNIST), N encysted samples (N=10,50,1000,2000) for each class, derived from our watermarking approach for the target model TM, are publicly



(a) Encysted samples for MNIST on the latent code that control the weight of digit (attribute-level disentanglement)



(b) Encysted samples for FFHQ on the texture latent codes

Figure 9: Visual Examples of few Encysted samples for fingerprinting on MNIST and FFHQ datasets (abstraction-level disentanglement). The first row is original reference samples, second and last row is the inner (same prediction with the reference) and outer (different prediction) encysted samples, respectively, as close to the decision boundary.

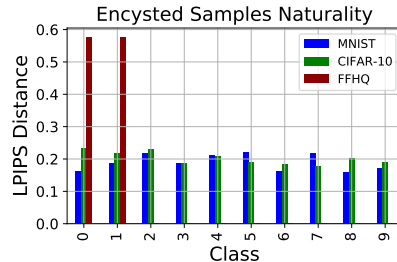


Figure 10: Naturality of encysted samples for fingerprinting among different classes.

released. And then the adaptive adversaries combine these watermarking samples into the training data in order to construct the compressed model TM' . Next, our watermarking approach is used to generate new encysted samples to distinguish TM' from TM . We demonstrate that the detection accuracy for TM' is not affected after applying adversarial training with different amounts of publicly released encysted samples. The reason for this may be uncertainty and randomness in the generation of encysted samples. The released augmented encysted samples could be regarded as randomly sampled points distributed around uncertain areas of the decision boundary of the target model, which is not effective for changing the decision boundary during adversarial training. On the other hand, we also test the performance of Sensitive Sample with

the same settings. The results indicate that the detection accuracy sharply decreases when the network is trained with sensitive samples along with their clean pairs. Based on adversarial training with $N=1000$, the attacked model could bypass more than 80% of sensitive samples, resulting in a similar performance to the randomly selected training samples. In other words, the adversarial training has successfully learned the distribution of fingerprinting samples created by Sensitive Samples.

5 Discussion

5.1 Efficiency and scope

Towards addressing the challenges of *Practicality* (w.r.t. *Feasibility, Randomness and low cost, Uncertainty and Sufficiency*), *Limited knowledge for design* (w.r.t. *Double-black-box*) and *Imperceptible* (w.r.t. *Generative model*), our algorithm can be characterized by the following five characteristics.

Feasibility and Randomness. As any sample can be augmented to a large number of encysted samples for effective verification of integrity, our PublicCheck is feasible even when a very small amount of training samples of the target model are available. The augmentation is a low-cost procedure via the feedforward neural network, leading to the feasibility of regularly checking the deployed model’s security status at runtime. Given the encysted noise range, encysted sample augmentation is conducted by adding randomly sampled perturbations to the disentangled latent codes.

Uncertainty. Linear perturbations in the latent space will result in non-linear structural change in the pixel space. These augmented encysted samples could be distributed over multiple parts of the decision boundary of the target model in an uncertain manner during each augmentation, instead of only one certain part for the adversarial example like watermarking. Besides, using multiple reference samples covering multiclass for random augmentation will help to prevent blind spots on the decision boundary. The uncertainty and randomness of the augmented encysted sample both benefit the public verification ability, even against pixel-wise adaptive attacks. We demonstrate this in Section 4.8.

Sufficiency. Due to the uncertainty, our experiments demonstrate that only five randomly selected encysted watermarking samples are required to achieve 100% verification and zero false-positive rate, without any extra coverage-guarantee mechanism. It means PublicCheck could achieve sufficient coverage for the model integrity verification without additional cost.

Double-black-box. Our PublicCheck made black-box access assumptions for both integrity inference and fingerprinting design, extending the scope to verify the integrity of black-box models such as encrypted models due to privacy concerns. Our PublicCheck is adaptive to redesign encysted samples for fingerprinting with only black-box access to the updated

models, without requiring fine-tuned models to be re-trained or parameters of these models to be updated.

Generative model. The quality of generative models and disentanglement strategies have direct impacts on the performance of the PublicCheck, especially quality of the augmented samples and the degree to which they appear natural. The naturality has been demonstrated to be satisfied even with moderate generative models and disentanglement strategies. More discussions are given in Section 5.3. The necessity of generative model is summarized as follows. First, as the watermarking samples could be visible for the adversary, the watermarking scheme operated in the pixel-space could always be bypassed by a strong adversary that also performs pixel-wise perturbation, as a Min-Max zero-sum game. Therefore, we conduct the watermarking scheme in the latent space of the generative model, aiming to defeat the adversary in the pixel space. Second, unlike the unstructured perturbation in the pixel space, our designed perturbation in the latent space is structured perturbation with reasonable controllability via the generative model and disentanglement strategies.

5.2 Once-off longevity and boosting strategies

Based on the uncertainty, randomness, and low-cost advantages, it is feasible to provide a once-off generation of encysted samples for fingerprinting via sampling random noise once. Namely, each generated encrypted sample for fingerprinting will be assumed to be used only once, as the more times a sample is used, the higher chance an attacker can manipulate the watermarking sample for public verification. Theoretically, an infinite number of perturbations could be sampled from the fixed encysted noise range for the fixed latent code of fixed size of reference original samples, producing infinite encysted samples. As the encysted sample for fingerprinting would be filtered via the naturality evaluation, the number of watermarking samples may not be infinite. However, the amount could still be further boosted towards infinity via combining existing latent codes (e.g., select two or more latent codes simultaneously to add the same or various perturbations), or extending the dimension of the latent representation, or assuming different noise distributions. Our experiments demonstrated that both single latent code perturbation (which requires careful analysis) and multiple (which does not) perform well. As only five encysted samples are enough to achieve 100% verification accuracy and the cost of verification may not be free (verification service is associated with API service purchase), the PublicCheck scheme is not practical to be broken even in public scenarios.

5.3 Limitations

The bottleneck of PublicCheck lies in the generative model and disentanglement strategies, both of which are open research questions for the machine learning community. Even

some state-of-the-art approaches, aimed at enhancing generative ability and disentanglement, could be incorporated into the PublicCheck scheme, we apply the moderate generative models and disentanglement strategies in this paper to explore the feasibility of our approach when the ability of generative models is limited. We will directly benefit from any future research progress in these areas. The performance of the generative models will increase when rising the fraction of the data for training. One promising solution to loosen the assumption on the amount of public available data to train the generative model is the data augmentation, such as Differentiable Augmentation (DiffAugment) [53], where the performance of the model trained using only 100 images for augmentation could match that trained on the entire dataset. How to leverage the data augmentation and transfer learning to address the assumption on public available data will be one of our next step studies.

6 Conclusion

We propose a practical DNN watermarking scheme PublicCheck, for ensuring the integrity of cloud-held models with public verifiability. The intuition of PublicCheck is to consider the inherent fingerprinting of a model as its decision boundary on the training dataset. In general, we create augmented samples on ordinary reference instances around the decision boundary of the target model by leveraging generative deep neural networks. Then, we select candidates that can capture some inherent behavior of the model as fingerprinting according to the watermarking efficiency and naturality criteria. It enables verification of the integrity in a low-cost and public manner based on the advantages of feasibility, randomness, uncertainty, and sufficiency, only using the black-box access during both inference and design procedures. Our experiments on both model integrity attacks and compression demonstrate that PublicCheck could address the practicality, imperceptible, and limited knowledge challenges.

References

- [1] ABUADBBA, A., KIM, H., AND NEPAL, S. Deepisign: invisible fragile watermark to protect the integrity and authenticity of cnn. In *Proceedings of the 36th Annual ACM Symposium on Applied Computing* (2021), pp. 952–959.
- [2] ADI, Y., BAUM, C., CISSE, M., PINKAS, B., AND KESHET, J. Turning your weakness into a strength: Watermarking deep neural networks by backdooring. In *27th {USENIX} Security Symposium ({USENIX} Security 18)* (2018), pp. 1615–1631.
- [3] BENET, J. Ipfs-content addressed, versioned, p2p file system. *arXiv preprint arXiv:1407.3561* (2014).
- [4] BIGGIO, B., AND ROLI, F. Wild patterns: Ten years after the rise of adversarial machine learning. *Pattern Recognition* 84 (2018), 317 – 331.
- [5] BROCK, A., DONAHUE, J., AND SIMONYAN, K. Large scale gan training for high fidelity natural image synthesis. *arXiv preprint arXiv:1809.11096* (2018).

[6] BURGESS, C. P., HIGGINS, I., PAL, A., MATTHEY, L., WATTERS, N., DESJARDINS, G., AND LERCHNER, A. Understanding disentangling in *beta-vae*. *arXiv preprint arXiv:1804.03599* (2018).

[7] CHEN, X., LIU, C., LI, B., LU, K., AND SONG, D. Targeted backdoor attacks on deep learning systems using data poisoning. *arXiv preprint arXiv:1712.05526* (2017).

[8] COURBARIAUX, M., BENGIO, Y., AND DAVID, J.-P. Training deep neural networks with low precision multiplications. *arXiv preprint arXiv:1412.7024* (2014).

[9] DOLATABADI, H. M., ERFANI, S., AND LECKIE, C. Advflow: Inconspicuous black-box adversarial attacks using normalizing flows. *arXiv preprint arXiv:2007.07435* (2020).

[10] FRIDRICH, J., AND GOLJAN, M. Robust hash functions for digital watermarking. In *Proceedings International Conference on Information Technology: Coding and Computing (Cat. No. PR00540)* (2000), IEEE, pp. 178–183.

[11] GAO, Y., XU, C., WANG, D., CHEN, S., RANASINGHE, D. C., AND NEPAL, S. Strip: A defence against trojan attacks on deep neural networks. In *Proceedings of the 35th Annual Computer Security Applications Conference* (2019), pp. 113–125.

[12] GHODSI, Z., GU, T., AND GARG, S. Safetynets: Verifiable execution of deep neural networks on an untrusted cloud. *arXiv preprint arXiv:1706.10268* (2017).

[13] GONG, Y., LIU, L., YANG, M., AND BOURDEV, L. Compressing deep convolutional networks using vector quantization. *arXiv preprint arXiv:1412.6115* (2014).

[14] GOODFELLOW, I., POUGET-ABADIE, J., MIRZA, M., XU, B., WARDE-FARLEY, D., OZAIR, S., COURVILLE, A., AND BENGIO, Y. Generative adversarial nets. In *Advances in neural information processing systems* (2014), pp. 2672–2680.

[15] GOODFELLOW, I. J., SHLENS, J., AND SZEGEDY, C. Explaining and harnessing adversarial examples. *arXiv preprint arXiv:1412.6572* (2014).

[16] GU, T., DOLAN-GAVITT, B., AND GARG, S. Badnets: Identifying vulnerabilities in the machine learning model supply chain. *arXiv preprint arXiv:1708.06733* (2017).

[17] HAN, S., MAO, H., AND DALLY, W. J. Deep compression: Compressing deep neural networks with pruning, trained quantization and huffman coding. *arXiv preprint arXiv:1510.00149* (2015).

[18] HE, K., ZHANG, X., REN, S., AND SUN, J. Deep residual learning for image recognition. In *Proceedings of the IEEE conference on computer vision and pattern recognition* (2016), pp. 770–778.

[19] HE, Z., ZHANG, T., AND LEE, R. Sensitive-sample fingerprinting of deep neural networks. In *Proceedings of the IEEE/CVF Conference on Computer Vision and Pattern Recognition* (2019), pp. 4729–4737.

[20] IANDOLA, F. N., HAN, S., MOSKEWICZ, M. W., ASHRAF, K., DALLY, W. J., AND KEUTZER, K. SqueezeNet: Alexnet-level accuracy with 50x fewer parameters and < 0.5 mb model size. *arXiv preprint arXiv:1602.07360* (2016).

[21] KARRAS, T., LAINE, S., AND AILA, T. A style-based generator architecture for generative adversarial networks. In *Proceedings of the IEEE Conference on Computer Vision and Pattern Recognition* (2019), pp. 4401–4410.

[22] KARRAS, T., LAINE, S., AITTALA, M., HELLSTEN, J., LEHTINEN, J., AND AILA, T. Analyzing and improving the image quality of stylegan. *arXiv preprint arXiv:1912.04958* (2019).

[23] KIM, H., AND MNIIH, A. Disentangling by factorising. *arXiv preprint arXiv:1802.05983* (2018).

[24] KRIZHEVSKY, A. Learning multiple layers of features from tiny images. Tech. rep., 2009.

[25] KURAKIN, A., GOODFELLOW, I., AND BENGIO, S. Adversarial machine learning at scale. *arXiv preprint arXiv:1611.01236* (2016).

[26] LECUN, Y., BOTTOU, L., BENGIO, Y., HAFFNER, P., ET AL. Gradient-based learning applied to document recognition. *Proceedings of the IEEE* 86, 11 (1998), 2278–2324.

[27] LI, Y., LI, L., WANG, L., ZHANG, T., AND GONG, B. Nattack: Learning the distributions of adversarial examples for an improved black-box attack on deep neural networks. In *International Conference on Machine Learning* (2019), PMLR, pp. 3866–3876.

[28] LIAO, C., ZHONG, H., SQUICCIARINI, A., ZHU, S., AND MILLER, D. Backdoor embedding in convolutional neural network models via invisible perturbation. *arXiv preprint arXiv:1808.10307* (2018).

[29] LIAO, F., LIANG, M., DONG, Y., PANG, T., HU, X., AND ZHU, J. Defense against adversarial attacks using high-level representation guided denoiser. In *Proceedings of the IEEE Conference on Computer Vision and Pattern Recognition* (2018), pp. 1778–1787.

[30] LIU, Y., XIE, Y., AND SRIVASTAVA, A. Neural trojans. In *2017 IEEE International Conference on Computer Design (ICCD)* (2017), IEEE, pp. 45–48.

[31] MA, S., LIU, Y., TAO, G., LEE, W.-C., AND ZHANG, X. Nic: Detecting adversarial samples with neural network invariant checking. In *Proceedings of the 2018 Network and Distributed Systems Security Symposium (NDSS), 2019. [Online]*. (2019).

[32] MA, X., LI, B., WANG, Y., ERFANI, S. M., WIJEWICKREMA, S., SCHOENEBECK, G., SONG, D., HOULE, M. E., AND BAILEY, J. Characterizing adversarial subspaces using local intrinsic dimensionality. *arXiv preprint arXiv:1801.02613* (2018).

[33] MEI, S., AND ZHU, X. Using machine teaching to identify optimal training-set attacks on machine learners. In *Twenty-Ninth AAAI Conference on Artificial Intelligence* (2015).

[34] MENG, D., AND CHEN, H. Magnet: a two-pronged defense against adversarial examples. In *Proceedings of the 2017 ACM SIGSAC Conference on Computer and Communications Security* (2017), ACM, pp. 135–147.

[35] MOOSAVI-DEZFOOLI, S.-M., FAWZI, A., AND FROSSARD, P. Deepfool: a simple and accurate method to fool deep neural networks. In *Proceedings of the IEEE Conference on Computer Vision and Pattern Recognition* (2016), pp. 2574–2582.

[36] NAGAI, Y., UCHIDA, Y., SAKAZAWA, S., AND SATOH, S. Digital watermarking for deep neural networks. *International Journal of Multimedia Information Retrieval* 7, 1 (2018), 3–16.

[37] OORD, A. v. d., VINYALS, O., AND KAVUKCUOGLU, K. Neural discrete representation learning. *arXiv preprint arXiv:1711.00937* (2017).

[38] PANG, R., ZHANG, Z., GAO, X., XI, Z., JI, S., CHENG, P., AND WANG, T. Trojanzoo: Everything you ever wanted to know about neural backdoors (but were afraid to ask). In *arXiv Preprint* (2020).

[39] PAPERNOT, N., McDANIEL, P., JHA, S., FREDRIKSON, M., CELIK, Z. B., AND SWAMI, A. The limitations of deep learning in adversarial settings. In *Security and Privacy (EuroS&P), 2016 IEEE European Symposium on* (2016), IEEE, pp. 372–387.

[40] PEI, K., CAO, Y., YANG, J., AND JANA, S. Deepxplore: Automated whitebox testing of deep learning systems. In *Proceedings of the 26th Symposium on Operating Systems Principles* (2017), ACM, pp. 1–18.

[41] RAZAVI, A., VAN DEN OORD, A., AND VINYALS, O. Generating diverse high-fidelity images with vq-vae-2. In *Advances in neural information processing systems* (2019), pp. 14866–14876.

[42] SHOKRI, R., STRONATI, M., SONG, C., AND SHMATIKOV, V. Membership inference attacks against machine learning models. In *2017 IEEE Symposium on Security and Privacy (SP)* (2017), IEEE, pp. 3–18.

[43] SIMONYAN, K., AND ZISSERMAN, A. Very deep convolutional networks for large-scale image recognition. *arXiv preprint arXiv:1409.1556* (2014).

[44] TURNER, A., TSIPRAS, D., AND MADRY, A. Clean-label backdoor attacks.

[45] UCHIDA, Y., NAGAI, Y., SAKAZAWA, S., AND SATOH, S. Embedding watermarks into deep neural networks. In *Proceedings of the 2017 ACM on International Conference on Multimedia Retrieval* (2017), ACM, pp. 269–277.

[46] W, X., D, E., AND Y, Q. Feature squeezing: Detecting adversarial examples in deep neural networks. in *Proceedings of the 2018 Network and Distributed Systems Security Symposium (NDSS), 2018. [Online]*. Available: <https://github.com/mzweilin/EvadeML-Zoo> (2018).

[47] WANG, B., YAO, Y., SHAN, S., LI, H., VISWANATH, B., ZHENG, H., AND ZHAO, B. Y. Neural cleanse: Identifying and mitigating backdoor attacks in neural networks. In *2019 IEEE Symposium on Security and Privacy (SP)* (2019), IEEE, pp. 707–723.

[48] WATANABE, S. Information theoretical analysis of multivariate correlation. *IBM Journal of research and development* 4, 1 (1960), 66–82.

[49] WIERSTRA, D., SCHAUL, T., GLASMACHERS, T., SUN, Y., PETERS, J., AND SCHMIDHUBER, J. Natural evolution strategies. *The Journal of Machine Learning Research* 15, 1 (2014), 949–980.

[50] Y, L., S, M., Y, A., W.-C, L., J, Z., W, W., AND X, Z. Trojaning attack on neural networks. in *25nd Annual Network and Distributed System Security Symposium, NDSS* (2018).

[51] ZHANG, J., GU, Z., JANG, J., WU, H., STOECKLIN, M. P., HUANG, H., AND MOLLOY, I. Protecting intellectual property of deep neural networks with watermarking. In *Proceedings of the 2018 on Asia Conference on Computer and Communications Security* (2018), ACM, pp. 159–172.

[52] ZHANG, R., ISOLA, P., EFROS, A. A., SHECHTMAN, E., AND WANG, O. The unreasonable effectiveness of deep features as a perceptual metric. In *CVPR* (2018).

[53] ZHAO, S., LIU, Z., LIN, J., ZHU, J.-Y., AND HAN, S. Differentiable augmentation for data-efficient gan training. *arXiv preprint arXiv:2006.10738* (2020).

Appendices

A Autoencoder based Generative Models

This section provides the necessary preliminaries to understand variational autoencoder and vector quantized (VQ) based generative models.

A.1 Variational autoencoder (VAE)

VAEs are a type of generative models that learn data representations by jointly training a probabilistic encoder and decoder network. We are attempting to develop representations that encode distinct attributes of the data into separate latent codes. Architecturally, the VAE-based generative models consist of two deep neural network components: the encoder E and decoder D. The encoder E maps the input $x \in \mathbb{R}^d$ to z in the latent space, to represent high-dimensional data through the low-dimensional latent representation, a.k.a. latent codes. The decoder D reconstructs z to the pixel space. The training

process of AE-based generative models is to minimize the reconstruction error and other restriction terms. In VAEs, the hypothesis is that the data is generated by a directed graphical model $p(x|z)$ and the encoder is to learn an approximation $q_\phi(z|x)$ to the posterior distribution $p_\theta(z|x)$. The VAE optimizes the variational lower bound:

$$L(\theta, \phi; x) = KL(q_\phi(z|x) || p_\theta(z)) - \mathbf{E}_{q_\phi(z|x)}[\log p_\theta(x|z)] \quad (8)$$

The left part is the regularization term to match the posterior of z conditional on x , i.e., $q_\phi(z|x)$, to a target distribution $p_\theta(z)$ by the KL divergence. The right part denotes the reconstruction loss for a specific sample x . In a training batch, the loss can be averaged as:

$$L_{VAE} = \mathbf{E}_{p_{data}(x)}[KL(q_\phi(z|x) || p_\theta(z))] - \mathbf{E}_{p_{data}(x)}[\mathbf{E}_{q_\phi(z|x)}[\log p_\theta(x|z)]] \quad (9)$$

The major drawback of existing disentangle-VAEs is that the disentanglement is achieved at the cost of reconstruction quality. Therefore, to improve the inner independence for good disentanglement among latent codes, Total Correlation (TC) [48] is applied to promote greater independence among the latent factors. The TC is formally defined as follow:

$$TC(z) = KL(q(z) || \bar{q}(z)) = Eq(z)[\log \frac{q(z)}{\bar{q}(z)}] \quad (10)$$

Since TC cannot be obtained directly, the approximate methods described in [23] are applied. In particular, a discriminator D_{TC} is used to estimate the probability $D(z)$. The input to D_{TC} is a sample from $q(z)$ rather than from $\bar{q}(z)$ in order to distinguish between samples from $q(z)$ and $\bar{q}(z)$. Consequently, it can approximate the density ratio for estimating TC [23]. D_{TC} , parameterized by ν , is trained with the encoder and decoder jointly. We substitute the TC term with the discriminator-based approximation as follows:

$$TC(z) \approx E_{q(z)}[\log \frac{D(z)}{1 - D(z)}] \quad (11)$$

The loss of VAE incorporated with a TC term is given as follows:

$$\frac{1}{N} \sum_N^{i=1} [E_{q_\phi(z|x^{(i)})}[\log p_\theta(x^{(i)}|z)] - D_{KL}(q_\phi(z|x^{(i)}) || p(z))] - \nu TC(z) \quad (12)$$

Generally, simple element-wise metrics, e.g., the pixel-wise squared error, are commonly adopted for the reconstruction error L_R . However, we focus more on the naturality of the reconstructed instances. Therefore, the similarity evaluation between input and reconstruction is desired to have the properties of human visual perception. Namely, what we would expect is the perceptual evaluation that measures how similar are two images in a way that coincides with human judgment. Consequently, we adopt a human perceptual evaluation of the images to measure the similarity. Namely, we replace the default pixel-wise reconstruction evaluation with the perceptual evaluation metric Learned Perceptual Image Patch Similarity (LPIPS) [52]. LPIPS is calculated as a weighted difference

between two VGG16 embeddings, where the weights are fit so that the metric agrees with human perceptual similarity judgments. During training, the VAE parameters are updated according to Eq. 12. The discriminator D_{TC} (e.g., an MLP classifier) is trained to classify between samples from $q(z)$ and $\bar{q}(z)$, based on the cross-entropy loss.

A.2 VQ based Generative Model

Generally, the vector quantized (VQ)-based autoencoder consists of three components, encoder En , decoder De , and codebook C . The codebook C can be considered as the common feature dictionary shared between the encoder and decoder. Namely, the codebook defines the commonly-shared latent embedding space $C \in R^{K \times D}$, consisting of K categorical embedding items with D dimension, i.e., $C_i \in R^D$, $i \in \{1, 2, \dots, K\}$. The encoder is a non-linear mapping from the input instance x in the pixel space the latent representation $z_e(x) \in R^{W \times H \times D}$, namely, $W \times D$ latent embedding vectors with D dimension ($z_e^{(i,j)} \in R^D$, $i \in \{1, 2, \dots, W\}$, $j \in \{1, 2, \dots, D\}$). Then, the latent representation $z_e(x)$ is further mapped to a discrete latent matrix $z^{(i,j)} \in R^1$, $i \in \{1, 2, \dots, W\}$, $j \in \{1, 2, \dots, D\}$. Here, each $z^{(i,j)}$ is the index of the nearest embedding items C_{nrs} in the codebook for each $z_e^{(i,j)}$ via nearest neighbour searching $\text{argmin}_m \|z_e^{(i,j)}(x) - C_m\|$, also called Vector Quantized, as demonstrated in Figure 5. The decoder reconstructs back to pixel space using the queried embedding items ($z_q(z)$) corresponding to the discrete latent index matrix via another non-linear function. The trainable parameters for the model are the union of parameters of the encoder, decoder, and the codebook. The overall loss function is given in Eq. 13

$$\begin{aligned} \mathcal{L}(x, De(z_q)) = & \text{Dist}(x - De(z_q)) + \|\text{sg}[En(x)] - C_{nrs}\|_2^2 \\ & + \beta \|\text{sg}[C_{nrs}] - En(x)\|_2^2 \end{aligned} \quad (13)$$

The operator sg refers to a stop-gradient operation that blocks gradients from flowing into its argument, and β is a hyper-parameter to control the reluctance to change the code corresponding to the encoder output.

There are three loss terms in Eq. 13 implemented to train different components of the VQ-based autoencoder. Specifically, the first term is the gradient of the reconstruction error $\text{Dist}(x - De(z_q))$, which will be back-propagated through the decoder, and to the encoder using the straight-through gradient estimator. Here, we replace the default pixel-wise reconstruction evaluation with the perceptual evaluation metric Learned Perceptual Image Patch Similarity (LPIPS) [52]. Besides, two additional terms are applied in the loss function to align the codebook’s embedding items with the encoder’s output. The codebook loss, which only applies to the codebook variables, brings the selected codebook close to the output of the encoder. The commitment loss, which only applies to the encoder weights, encourages the output of the encoder to

stay close to the chosen codebook vector to prevent it from fluctuating too frequently from one code vector to another. The exponential moving average updates are used to update the codebook, as a replacement for the codebook loss (the second loss term in Eq. 13):

$$\begin{aligned} N_i^{(t)} := & N_i^{(t-1)} * \gamma + n_i^{(t)}(1 - \gamma), \quad m_i^{(t)} := m_i^{(t-1)} * \gamma \\ & + \sum_j^{n_i^{(t)}} E(x)_{i,j}^{(t)}(1 - \gamma), \quad e_i^{(t)} := \frac{m_i^{(t)}}{N_i^{(t)}} \end{aligned} \quad (14)$$

Here, $n_i^{(t)}$ is the number of vectors in $E(x)$ in the mini-batch quantized to codebook item C_i at timestamp t , and γ is a decay parameter with a value between 0 and 1 (default 0.99).

Although the training time of VQ generative model takes hours for 256x images, that is a once-off procedure on the server-side that could be carried out in parallel across several GPUs or by using the pre-trained model for transfer learning to further reduce the training time. Besides, the generative could be reused for the similar datasets, e.g. the model pre-trained on the FFHQ face dataset could be used for other human face datasets.

B Datasets and Settings

Here, we provide more details about the three datasets and three DNN model architectures we use. (1) MNIST consists of 28x28 grayscale handwritten digit images from 10 classes, i.e., digit 0-9, and has a training set of 55000 instances and a test set of 10000 instances. (2) The CIFAR-10 dataset consists of 60000 32x32 color images in 10 classes, with 6000 images per class, including airplane, automobile, bird, cat, deer, dog, frog, horse, ship, and truck. (3) To evaluate the effectiveness of our watermarking approach on a dataset of a larger class number, we also used the CIFAR-100 dataset. This dataset contains 100 classes containing 600 images each. The 100 classes in the CIFAR-100 are grouped into 20 superclasses. The images are resized to 64px in our experiments. (4) Flickr-Faces-HQ (FFHQ) is a high-quality image dataset of human faces, consisting of 70,000 high-quality 1024x1024 resolution images from Flickr and associated with considerable variation in terms of age, ethnicity, and image background. The images are resized to 256px in our experiments.

Table 4: Classification model used for each of the datasets and their baseline accuracy.

Dataset	Task	Model	Accuracy
MNIST	Digit Classification	LeNet	99.97
CIFAR-10	Image Classification	ResNet18	93.59
FFHQ	Gender Classification	VGG16	89.87

The target classifier for MNIST using the LeNet, consisting of three sets of convolution layers with a combination of average pooling, followed by two fully connected layers. At last, a Softmax function which classifies the images into respective class. For the CIFAR-10 data, the target classifier

is adopted the ResNet-18 [18], consisting of 18 convolutional layers utilizing skip connections or shortcuts to jump over some layers to address vanishing gradients. For the FFHQ data, the target classifier is used the VGG-16 [43], consisting of 16 convolutional and fully connected layers mostly have 3×3 filters. Table 4 shows the classification models used in our experiments for each of these datasets, and the corresponding model accuracy.

Our DNN techniques are implemented using PyTorch, backdoor attacks are deployed in the TrojanZoo [38] platform, and the PublicCheck in Python. The number of instances that are randomly sampled as reference samples is generally 3-4 times of required number of the encysted sample for fingerprinting. For example, if four encysted samples for fingerprinting are desired, accordingly, we randomly select 20 reference samples to conduct augmentation, followed by randomly selecting 4 augmented encysted samples that satisfied the naturality. Each entry in the results of performance for watermarking is averaged over 1000 repetitions of augmentation and selection.

C Architectures and Hyperparameters

The VAE-based generative model (attribute-level disentanglement) is used for MNIST, and the architecture and hyperparameters are similar to the settings in [23]. The encoder consists of four strided convolutional layers with steps of 2 and a window size of 4×4 , followed by two fully connected layers with 128, 2*10 hidden units respectively. In the decoder, there are one fully connected layers (128 hidden units), followed by four transposed convolutions with stride 2 and window size 4×4 . The VQ-based generative model(abstraction-level disentanglement) is used for CIFAR and FFHQ. As the CIFAR-10 images are with low fidelity, we combine the top and bottom encoder into one, i.e. the ordinary VQ-based autoencoder in Appendix A.2 is used. The architecture and hyperparameters of the ordinary VQ-based autoencoder are similar to the settings in [37] and that of two-encoder VQ-based generative model (abstraction-level disentanglement) for FFHQ are similar to the settings in [41]. The encoder consists of two strided convolutional layers with steps of 2 and a window size of 4×4 , followed by two residual 3×3 blocks (implemented as ReLU, 3x3, ReLU, 1x1), all of which have 128 hidden units. In the decoder, there are two residual 3×3 blocks, followed by two transposed convolutions with stride 2 and window size 4×4 . Default hyperparameters are summarized in the following table.

Table 5: Default Hyperparameter Settings

Parameter	Default Value (MNIST, CIFAR-10, FFHQ)
Input size	28,256,256
β	-,0.25,0.25
Batch size	16,128,128
Codebook size	-, (k=512, d=64), bottom (k=512, 64)+top (k=256, d=32)
Training steps	50, 25000,25000
Learning rate	1e-4, 2e-4, 2e-4

D Visualization of Sensitive Samples and Backdoor Attacks

A fingerprinting instance is generally created from an original example by adding a trigger or pixel perturbation in existing works. In this section, we demonstrate that such pixel-level fingerprinting patterns can be distinguished by human perception in Figure 11 and 12.



Figure 11: Visualization of Sensitive Samples [19] for private verification of model integrity (Second row). First row is the corresponding original images.



Figure 12: Visualization of triggers (Trojan Square and Trojan Watermark) used in Backdoor attacks [50]

E MLaaS and Relevant DNN Attacks

Deep Neural Networks (DNNs) are computationally intensive and are composed of numerous parameters that require extensive training on large datasets. Therefore, cloud-enabled services have become a natural choice for developing and deploying DNNs. This has encouraged many of the giant technology companies with elastic cloud to offer Machine Learning as a Service (MLaaS) on their cloud platforms, e.g., Google Vertex AI ¹, Amazon machine learning ², Microsoft Azure machine learning ³, IBM Watson studio ⁴ and Bigml ⁵.

These platforms provide simple APIs for: (1) uploading entire datasets and perform model training on the cloud, or (2) data owners upload models only after training them locally for sensitivity reasons. The later is offered recently by many platforms for data owners to deploy their pre-trained models and then share it with others(customers) through the cloud platform's API for profits. The details of the running models are hidden from both data owners and the customers. For

¹<https://cloud.google.com/vertex-ai>

²<https://aws.amazon.com/machine-learning/>

³<https://azure.microsoft.com/>

⁴<https://www.ibm.com/au-en/cloud/watson-studio>

⁵<https://bigml.com/>

instance, Google Prediction API hides all details, while Amazon ML provides only a limited set of options [42]. Service providers gain revenue by charging customers for queries through API only. Therefore, MLaaS prediction APIs are mostly a black-box service.

While promising, the MLaaS model (and outsourced models, in general) poses critical security concerns, specifically relating to the integrity of the served model by the cloud provider at the time of queries. Here are a few examples of those potential attacks:

Model Compression attack. The attacker’s (cloud provider’s) aim is to compress the DNN model with negligible accuracy reduction, to minimize required cloud storage for profit. Examples of compression techniques that may achieve this are quantization [13], pruning [17], low precision [8] and architecture optimization [20]. In the later one, the service provider may use single-layer instead of a multi-layer neural network, to minimize its computational costs [12].

Neural network trojan attack the cloud provider could be compromised by malware that injects a trojan into the model so that the model misclassifies samples containing a specific trigger [16, 50].

Targeted poisoning attack It is an attack in which the attacker retrains the model by using at least one sample and corresponding label (not reflecting the ground truth) [33] to force the model to misclassify.

Model Poisoning Defenses: Many defense works have been introduced in the literature to defeat backdoor or model poisoning attacks. Liu et al. [30] proposed several defense mechanisms: (i) anomaly detection over training data: such a method requires access to the poisoned dataset, which might not be realistic in practice; (ii) Removing the backdoors by retraining: while it is effective to some extent but continuous retraining might be an expensive task and would not guarantee the complete removal of backdoors as demonstrated by previous work in [16]; (iii) Focusing on removing the trigger by preprocessing the input data – it might capture a certain percentage of the attacks but does not guarantee to eliminate the backdoor risk within the model itself. Liu et al. [50] further proposed a backdoor detection by examining the distribution of mislabelled data. However, the success of this assumption requires the victim to feed the model with a relatively large dataset of samples, rendering such an approach inefficient and expensive. Despite being robust, these defense techniques assume full access to the model during the verification and lack a mechanism to track the integrity in black-box setting. That is, how model users, in the MLaaS and relevant integrity attacks scenario, can remotely ensure continuous integrity of the offered model?

Adversarial Samples: Another active related stream of work worth to be discussed is adversarial samples [4]. The focus of this stream is not poisoning the model itself but rather manipulating the input data in such a way that lead clean DNN models to misclassification at the testing time.

Attacks: Fast gradient sign method by Goodfellow et al. [15], basic iterative method by Kurakin et al. [25], DeepFool by Moosavi et al. [35], Jacobian-based Saliency map method by Papernot et al. [39], and DeepXplore method by Pei et al. [40] are a few examples of these attacks. **Defenses:** Adversarial sample detection mechanism is a very active area of research. Examples include a statistical measurement using local intrinsic dimensionality by Ma et al. [32], performing denoiser process on the incoming input as in Magnet [34] and high representation denoiser by Liao et al. [29], feature squeezing mechanism to reduce the colour depth of images by Xu et al. [46], input filters, neuron pruning and unlearning by Wang et al. [47], perturbation based entropy by Gao et al. [11], and using network invariant checking by Shiqing et al. [31]. Our work is not designed to detect this type of attacks as the model is not touched and only adversarial samples are crafted externally.

Settings for implemented attacks. We summarize the default setting of the backdoor attacks used in our evaluation in Table 6.

Table 6: Attack default settings.

Attack	Parameters	Values
Trainining	learning rate	0.01
	retrain epoch	50
	optimizer	SGD
	momentum	0.9
	weight decay	2e-4
BadNet	poison_percent	0.1
TrojanNN	layer	logits
	neuron	2
	optimizer	PGD
	lr	0.015
	iter	20
Clean-Label	threshold	5
	target	10
	poison generation	PDG
	tau	0.4
	epsilon	0.1
	noise_dim	100
	iter	1000

F Blockchain and IPFS based Fingerprinting Images Management

In this section, we explore a potential management solution for encysted sample images based on blockchain and the InterPlanetary File System (IPFS).

Storage Step. Initially, the model owner registers basic information on the resource storage page, including the resource model ID, the name of the owner to which it belongs, the time, etc. Then, the PublicCheck module is called for encysted samples for fingerprinting using the black-box access to the model. The generated images are stored in IPFS, which is a protocol and peer-to-peer network for storing and sharing data in a distributed file system [3]. IPFS uses content-addressable block storage to uniquely identify each file within a global namespace connecting all computing devices. IPFS first hashes the produced images and uses the hash values (e.g.,

SHA256, RIPEMD160) as the file’s unique identification and address in the IPFS network. Once the file is stored in the IPFS network, the server only needs to store the file’s address in IPFS, which greatly reduces the storage overhead. Besides, since the address is found through the file’s hash, which will be changed when the file’s contents are maliciously tampered with. At the same time, these basic information provided by the owner, responded IPFS address, and timestamps, will be processed as fixed-length hex strings. These hex strings are then saved to the blockchain by using the smart contract.

Acquisition Step. Following the querying and browsing of the basic information about the resource, the end user may request information associated with API purchases and model deployments as identity information. The management system then invokes the associated smart contracts, reads the hash address in the basic information about files, and downloads the resource files stored in IPFS, without providing a user download interface. In addition, the user’s identity information is extracted and translated into a digital fingerprint code, which is then embedded in the resource file to create a resource file containing fingerprint information. After embedding, the public key in the fingerprint certificate is used to encrypt the resource file, and a download interface is provided to the user. The user downloads the resource file through the interface, and decrypts the resource file with the private key to obtain the digital resource embedded with fingerprint information. As encysted sample images could be once-off, an inventory threshold will be set to trigger a new round of generation.

G Existing Watermarking Works

It can be categorised based on the aim into (1) protecting the Intellectual Property (IP) of DNN models, and (2) protecting the integrity of the DNN models where our work belongs. (1) The former focuses on claiming the ownership of the models by developing a persistent watermark, but not protecting the model integrity as such answering the question — has the model been changed? In fact, the aim is the opposite; that is, trying to build a robust watermark that cannot be removed easily by model sealers. Examples include: embedding a small number of bits into deep layers by Uchide et al. [36, 45], infusing a verifiable watermark in black-box settings by Zang et al. [51], inserting a backdoor to claim the ownership by Adi et al. [2]. (2) The latter aims at protecting the integrity of the DNN models while being used. There are few works introduced so far. Abuadbba et al. [1] proposed a fragile watermark based mechanism but requires white-box access during verification. Recently, He et al. [19] introduced model fingerprinting that allows model integrity verification in black-box settings. However, their approach only allows verification by an honest party—they are only privately verifiable due to their technique limitations of lacking randomness/uncertainty, infinite generation, or imperceptibility. On the contrary, the MLaaS scenario has a large number of users that necessitates

the need for public verifiability with those characteristics. To the best of our knowledge, this is the first work to promote the public verification of model integrity towards practice by leveraging the advantages of feasibility, randomness, uncertainty, and sufficiency while only using black-box access during inference and design procedures.